

Electronic and magnetic transitions in a multiband model for La_2NiO_4

Priya Mahadevan

*Solid State and Structural Chemistry Unit, Indian Institute of Science, Bangalore-560 012, India
and Department of Physics, Indian Institute of Science, Bangalore-560 012, India*

K. Sheshadri

Institute of Mathematical Sciences, C.I.T. Campus, Madras-600113, India

D. D. Sarma*

Solid State and Structural Chemistry Unit, Indian Institute of Science, Bangalore-560 012, India

H. R. Krishnamurthy* and Rahul Pandit*

Department of Physics, Indian Institute of Science, Bangalore-560 012, India

(Received 2 December 1996)

The transition-metal oxide La_2NiO_4 is studied using a multiband Hubbard model with a Hund coupling J . We obtain its mean-field phase diagram in the U - (Δ correlation strength on Ni sites) (Δ charge-transfer energy) plane. For $J=0$ we have a continuous transition from a paramagnetic metal (PMM) to a paramagnetic insulator (PMI). On increasing J , the magnetic moment M and the band gap E_G change discontinuously at $J=J_c(U, \Delta)$. For $J=1$, the insulating phase (AFI) is antiferromagnetic, but we have, in addition, both paramagnetic (PMM) and antiferromagnetic (AFM) metallic phases. The insulator-metal (AFI-AFM and AFI-PMM) phase boundaries are first order, but the metal-metal (AFM-PMM) boundary is second order; and it seems to meet the first-order boundary at a critical end point. A reentrant PMM-AFM-PMM sequence is also seen. [S0163-1829(97)01316-7]

Considerable attention has been focused on cuprates and related oxides since the discovery¹ of high- T_c superconductivity. However, there is a large class of other, non-superconducting oxides with interesting electrical and magnetic properties, which have not received as much attention. This includes transition-metal oxides of the type ABO_3 and A_2BO_4 . Of particular interest is La_2NiO_4 , which is isostructural with La_2CuO_4 . On doping with a small amount of strontium, both compounds which are antiferromagnetic insulators lose their magnetic order. However, $\text{La}_{2-x}\text{Sr}_x\text{CuO}_4$ becomes a superconductor for a range of dopant concentrations, whereas $\text{La}_{2-x}\text{Sr}_x\text{NiO}_4$ continues to be an insulator for $x < 1$. In order to understand the unusual properties of $\text{La}_{2-x}\text{Sr}_x\text{NiO}_4$, a natural first step is to study the undoped parent compound, La_2NiO_4 , which is an insulator with a band gap of about 4 eV (Ref. 2) and orders antiferromagnetically with a moment $M \approx 1.8\mu_B$.³

The electronic structures of undoped transition-metal oxides have been traditionally discussed in terms of a phase diagram proposed by Zaanen, Sawatzky, and Allen (ZSA).⁴ This well-known ZSA phase diagram was established by extensive calculations for the electronic charge-excitation gaps within the Anderson impurity Hamiltonian for every possible d^n configuration. It separates the insulating regime from the metallic one by a second-order transition in the U - Δ plane. The use of a single transition-metal ion in the impurity model, however, precludes any possibility of describing the magnetic structure of the transition-metal compounds within this model. Hence a mean-field treatment of a multiband Hubbard model suitable for a square-planar CuO_2 lattice was employed⁵ to provide a description of both charge and spin

degrees of freedom. The resulting phase diagram established the existence of the *covalent insulating* regime, in addition to the other phases already identified by ZSA. However, the ZSA phase diagram⁴ and its modification⁵ are qualitatively similar, to the extent that a single continuous phase transition separates the insulating and the metallic states.

Here we show that the phase diagram for a multiband model for La_2NiO_4 is *qualitatively different* from ZSA-type phase diagrams in that it exhibits first- as well as second-order electronic transitions and even a reentrant magnetic transition. Thus the La_2NiO_4 class displays a much wider range of behaviors than the La_2CuO_4 class,⁵ though they are isostructural. This result emphasizes the importance of accounting for electronic configurations and electronic interaction parameters in determining the topology of the phase diagram.⁶

In order to describe the d^8 electron configuration in a multiband Hubbard model, we must include an additional term in the Hamiltonian. This is the Hund coupling J that favors the state with the maximum local spin. In La_2NiO_4 each nickel atom is surrounded by six oxygen atoms, which form a distorted octahedron, thus reducing the point-group symmetry from O_h to D_{4h} . This lifts the degeneracy of the $d_{3z^2-r^2}$ (a_{1g} symmetry) and $d_{x^2-y^2}$ (b_{1g} symmetry) levels. The other three Ni d levels, being fully filled, do not contribute to any physical properties. Thus we have two holes distributed between the a_{1g} and b_{1g} levels depending on the relative strengths of the crystal-field splitting and J in the ionic limit. We denote the state with two holes at the Ni site and no holes at the O sites by d^2L^0 . Taking note of the

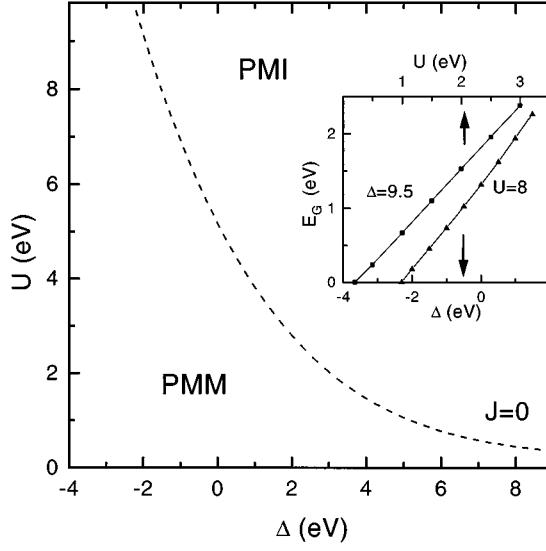


FIG. 1. The phase diagram in the U - Δ plane for $J=0$. The dashed line shows the continuous (second-order) phase boundary between paramagnetic metal (PMM) and paramagnetic insulator (PMI) phases. The linear dependences of the band gap E_G on Δ , in the large- U regime, and on U , in the large- Δ regime, are shown in the inset.

strong two dimensionality of the crystal structure of La_2NiO_4 , we consider only the two-dimensional Ni-O plane, including the apical O atoms, so that each unit cell has one Ni and four O atoms.⁷ There are two relevant orbitals on the Ni and three on each O, resulting in 14 orbitals (28 spin orbitals) in each unit cell. Thus the Hamiltonian is

$$\begin{aligned}
 H = & \sum_{i,l,\sigma} \epsilon_p p_{il\sigma}^\dagger p_{il\sigma} + \sum_{i,l,\sigma} \epsilon_d^\dagger d_{il\sigma}^\dagger d_{il\sigma} \\
 & + \sum_{i,j,l_1,l_2,\sigma} t_{ij,pp}^{l_1 l_2} p_{il_1\sigma}^\dagger p_{jl_2\sigma} + \sum_{i,j,l_1,l_2,\sigma} t_{ij,pd}^{l_1 l_2} d_{il_1\sigma}^\dagger p_{jl_2\sigma} \\
 & + \sum_{i,l_1,l_2,\sigma,\sigma'} U d_{il_1\sigma}^\dagger d_{il_2\sigma'}^\dagger d_{il_2\sigma'} d_{il_1\sigma} - \sum_i J S_i^2, \quad (1)
 \end{aligned}$$

where $d_{il\sigma}^\dagger$ ($d_{il\sigma}$) creates (annihilates) a hole with spin σ in the l th d orbital ($l=1$ for x^2-y^2 and $l=2$ for $3z^2-r^2$) on the Ni atom at the i th site, $p_{il\sigma}^\dagger$ ($p_{il\sigma}$) creates (annihilates) a hole with spin σ in the l th p orbital ($l=1,2,3$ for x,y,z) on the O atom at the i th site, and S_i is the total spin of the Ni atom at the i th site. The last term in Eq. (1) is the Hund coupling which ensures that the state with $S=1$ is lower in energy than the one with $S=0$ in the atomic limit.

The various t_{pp} 's and t_{pd} 's were determined in terms of the usual Slater-Koster⁸ parameters t_{pp}^σ , t_{pp}^π , t_{pd}^σ , and t_{pd}^π . For the hopping strengths in the basal plane we used $t_{pd}^\sigma = 1.6$ eV, $t_{pp}^\sigma = -0.6$ eV, and $t_{pp}^\pi = 0.4$ eV, which are similar to the values obtained earlier from an analysis of band-structure results,⁹ the qualitative features of the various results presented here are, however, not very sensitive to the exact values used. The hopping interaction strengths were assumed to scale with distance (r) as $1/r^{l+l'+1}$ where l and l' are the angular momenta of the orbitals involved. The

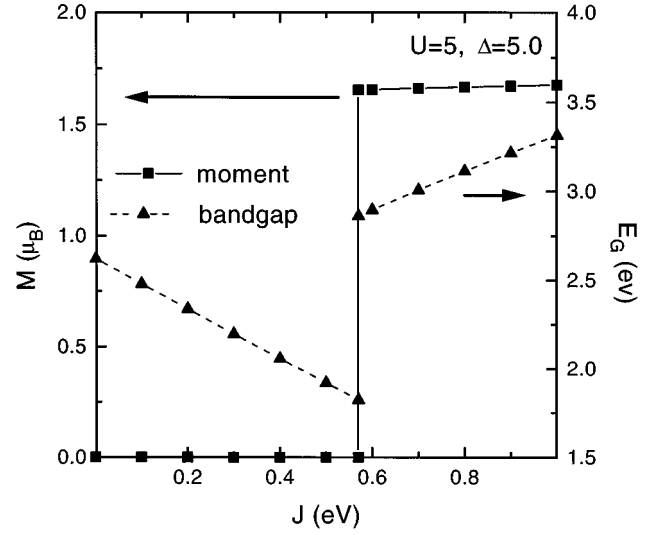


FIG. 2. The magnetic moment M versus J for $U=5$ eV and $\Delta=5$ eV. The jump at $J=J_c$ clearly indicates a first-order transition.

$d_{3z^2-r^2}$ orbitals have an on-site hole energy ($\epsilon_d^2 = \epsilon_{d_{3z^2-r^2}}$) 0.5 eV (Ref. 9) more than that ($\epsilon_d^1 = \epsilon_{d_{x^2-y^2}}$) of the $d_{x^2-y^2}$ orbitals because of crystal-field effects. The minimum energy required to transfer a hole from a nickel site to the oxygen site is the charge-transfer energy $\Delta = \epsilon_p - \epsilon_{d_{3z^2-r^2}} - U + J$.

We decoupled the four-fermion terms in model (1) by using a mean-field approximation⁵ and then solved self-consistently for the order parameters in \mathbf{k} space with 900 or 1600 points within the two-dimensional Brillouin zone, to ensure that our results were not affected by the finite resolution of the \mathbf{k} grid. The convergence criterion used was that the differences between the order parameters between successive iterations were less than 10^{-6} . The band structure of the effective one-electron problem, the band gap E_G , the ground-state energy, and various orbital and spin related order parameters were determined after the solution had converged. The energies of various possible electronic and magnetic states were obtained at a given set of values of U , Δ , and J . A comparison of the total energies of these states yielded the ground-state behavior at a given point in the U - Δ - J parameter space. Such calculations were performed at various points in the U - Δ space for two fixed values of J ($=0$ and 1 eV) to obtain the representative phase diagrams.

To ensure that the model (1) is indeed relevant for La_2NiO_4 and related compounds, we compare the physical properties of La_2NiO_4 , as calculated from our mean-field theory, with those obtained experimentally. The values of the other interaction parameters, namely, U and Δ , have been estimated from high-energy spectroscopies to be about 8 eV and 4 eV,² respectively. If we set $J=1$ eV,⁹ we find a band gap of about 4 eV and a magnetic moment $M \approx 1.7\mu_B$. The experimental band gap is ≈ 4 eV (Ref. 2), and the magnetic moment $M \approx 1.8\mu_B$,³ thus there is good agreement between our results and experiments.

In Fig. 1 we show the phase diagram in the U - Δ plane for $J=0$, with the inset illustrating typical variations of the gap as a function of Δ (for $U=8$) and U (for $\Delta=9.5$). In each

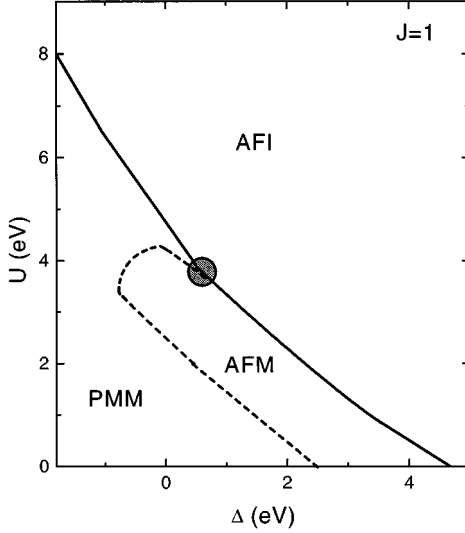


FIG. 3. The phase diagram in the U - Δ plane for $J=1.0$ eV showing antiferromagnetic insulator (AFI), antiferromagnetic metal (AFM), and paramagnetic metal (PMM) phases. Dashed lines indicate continuous (second-order) phase transitions and the solid line indicates a first-order boundary. These meet, in all likelihood (see text), at a critical end point (shaded circle).

case, the band gap is found to decrease continuously to zero, indicating that there is always a continuous transition between a paramagnetic insulator and a paramagnetic metal for $J=0$. The paramagnetic states, throughout the $J=0$ plane, are easy to understand, since, in the absence of the Hund rule (or *intraatomic* exchange) coupling, the crystal-field splitting always favors the $S=0$ state with spins paired at each site. The metal-insulator transition (MIT) in the phase diagram of Fig. 1 is qualitatively similar to the ZSA diagram⁴ or the modified-ZSA diagram,⁵ insofar as there is only one second-order phase boundary.

Since La_2NiO_4 is an antiferromagnetic insulator, which does not appear in the phase diagram of Fig. 1, we must allow for $J>0$ in model (1). We begin by investigating the effect of J on the band gap E_G and the magnetic moment M at the Ni site at a given point in the U - Δ plane, namely, $U=5$ eV and $\Delta=4.5$ eV. We find that both change discontinuously at a critical value, $J=J_c \approx 0.6$ eV (Fig. 2), signifying a first-order transition. The reason for the discontinuous changes as a function of J can be understood easily in the ionic limit. For small values of J , the two holes reside on the $d_{x^2-y^2}$ orbital giving rise to the $S=0$ state because of the finite crystal-field splitting. Once J becomes greater than the crystal-field splitting, the two holes adopt a parallel spin configuration ($S=1$) by distributing themselves equally in the $d_{x^2-y^2}$ and the $d_{3z^2-r^2}$ orbitals, with J more than compensating for the crystal-field splitting. This shows that the first-order transition between the paramagnetic $S=0$ state and the magnetic $S=1$ state occurs at $J_c = (\epsilon_d^2 - \epsilon_d^1) = 0.5$ eV in our model in the ionic limit. In the presence of hopping J_c changes somewhat, since the $d_{x^2-y^2}$ and $d_{3z^2-r^2}$ orbitals hybridize differently with the oxygen orbitals because of the distortions of the NiO_6 octahedron. However, J_c appears to depend only weakly on other electronic interaction param-

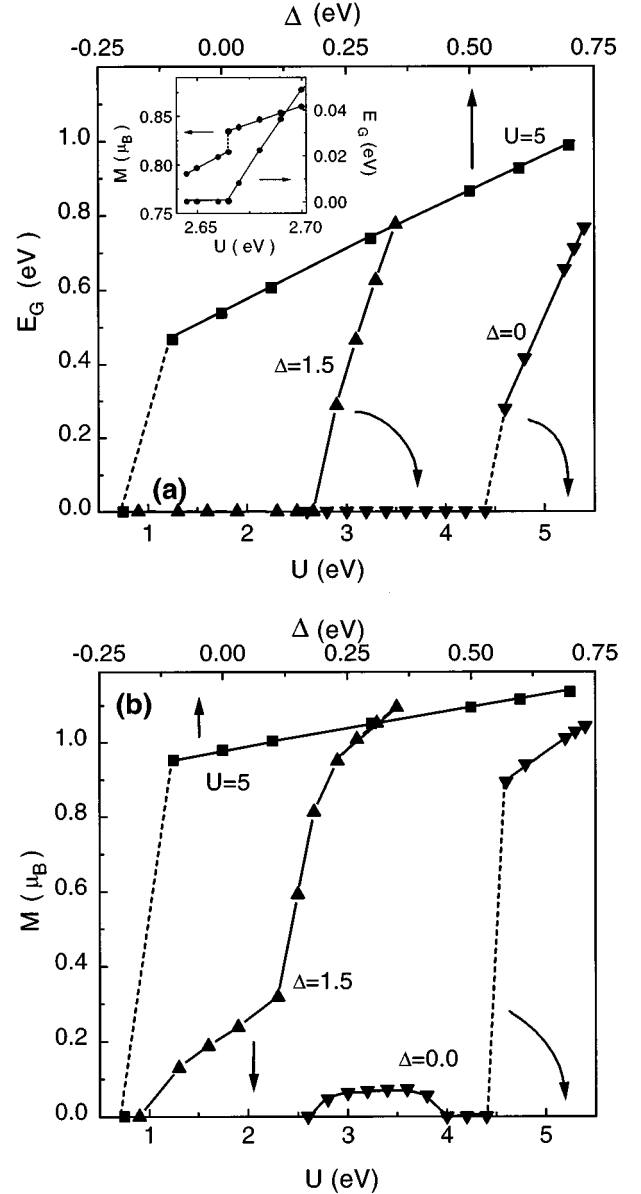


FIG. 4. Representative scans at fixed U or Δ showing the dependence of (a) E_G and (b) M on Δ (or U) for the cases $\Delta=1.5$ eV (full triangles), $\Delta=0$ eV (full inverted triangles), and $U=5$ eV (full squares). Continuous transitions are indicated by smooth variations in M and/or E_G and are marked by solid lines, while the first-order changes are marked with dashed lines. The inset in (a) shows the small discontinuity in the magnetic moment across the AFM-AFI phase transition for $\Delta=1.5$ eV.

eters, since $J_c \approx 0.6$ eV for the parameters of Fig. 2 and at various other points in the U - Δ plane not shown here.

In Fig. 3 we show the mean-field phase diagram of model (1) for $J=1$ eV. Note that it is qualitatively different from the phase diagram of Fig. 1 in that it shows a paramagnetic metal (PMM) phase and *two* antiferromagnetic phases, one an antiferromagnetic insulator (AFI) and the other an antiferromagnetic metal (AFM). The topology of this phase diagram is such that the metallic phases (PMM and AFM) are separated from the insulating phase (AFI) by a first-order phase boundary (solid line), whereas the phase transition between the metallic phases (AFM-PMM transition) is a con-

tinuous one (dashed line). The simplest way in which the first- and the second-order phase boundaries can meet is at a critical end point (shaded circle); however, such numerical studies are not accurate enough to rule out more complicated topologies with combinations of other multicritical points (like tricritical points), which might well arise from further-neighbor interactions. Note that the AFM-PMM phase boundary curves in a way that allows the reentrance sequence PMM-AFM-PMM with changing Δ or U over a limited range of our parameter space.

The phase diagram of Fig. 3 is based on various scans through the U - Δ plane which examine the variations of E_G and M with Δ at fixed U or vice versa. Three representative scans are shown in Figs. 4(a) and 4(b) for E_G and M , respectively. (1) For $\Delta = 1.5$ eV (full triangles), M [Fig. 4(b)] rises continuously from 0 at the PMM-AFM transition at $U \approx 0.9$ eV, but E_G [Fig. 4(a)] remains at 0 till $U \approx 2.7$ eV, signifying a second-order transition between the metallic states. For larger values of U , a finite band gap develops, indicating a metal-insulator transition [see Fig. 4(a)]. This transition between the metallic (AFM) and the insulating (AFI) phases is first order, though the resolution of the figure is not adequate to show the discontinuity. Therefore we have shown the variations in the moment and the band gap over a very narrow range of the parameter space near the transition point in the inset of Fig. 4(a). This clearly shows a discontinuous change in the moment at the transition point. We have checked the order of this AFM-AFI transition at several points along the phase boundary by carrying out similar calculations over very fine grids in the parameter space and have indeed confirmed that it is always a first-order transition. (2) For $\Delta = 0$ (full inverted triangles), we have a clear first-order PMM-AFI transition as can be seen from the jumps in both E_G [Fig. 4(a)] and M [Fig. 4(b)] at $U \approx 4.4$ eV. With decreasing U , we find that a finite moment develops for U less than about 4.0 eV [see Fig. 4(b)], but the band gap remains zero, indicating a transformation from the PMM to the AFM phase. Eventually M disappears for U less than about 2.6 eV, showing a reentrant PMM phase. Within our numerical accuracy, the PMM-AFM boundary appears to be

second order. (3) If we increase Δ at $U = 5$ eV (full squares), we only encounter the first-order PMM-AFI transition at $\Delta \approx -0.23$ eV.

It is worth noting that our phase diagram (Fig. 3) exhibits all categories of insulators discussed in the ZSA and modified-ZSA contexts,^{4,5} namely, charge-transfer, Mott-Hubbard, and covalent insulators (see the variation of E_G in the inset of Fig. 1). In addition, our model (1) also shows a Slater insulator at $U = 0$ for $\Delta > 4.7$ eV; this is made possible by the presence of a finite J in the system.

To summarize, our study of La_2NiO_4 shows that a two-dimensional, multiband Hubbard Hamiltonian can describe the low-energy physics of the undoped compound if we include the Hund coupling. We have shown this yields quantitative agreement between experimental and calculated band gaps and the magnetic moment. The U - Δ phase diagram for $J = 0$ shows a continuous transition between PMI and PMM phases. This topology persists for $0 < J \leq J_c$. For $J > J_c$ the phase diagram is *qualitatively* different from the ZSA type.^{4,5} Specifically, for $J = 1$ eV, the phase diagram shows an AFI phase for large U and Δ , which persists even for $U = 0$ when $\Delta \geq \Delta_c \approx 4.7$ eV. AFM and PMM phases also appear in this phase diagram, which has a rich topology including first-order and continuous phase boundaries meeting at a critical end point. The phase diagram also shows an intriguing PMM-AFM-PMM reentrant sequence for small values of Δ . Thus the electronic and magnetic phase diagrams for transition-metal compounds of the A_2BO_4 type are determined not only by the various electronic strengths, but also depend explicitly on the electron configuration and lattice geometry. It would be interesting to see if phase diagrams like Fig. 3 can be obtained by studying a whole class of such oxides, each member of which will be characterized by different coupling strengths¹⁰ in model (1), although it might be hard to resolve the topologies of such phase diagrams near multicritical points.

We thank UGC and CSIR (India) for support and the SERC (IISc, Bangalore) for providing us with computational facilities.

*Also at Jawaharlal Nehru Centre for Advanced Scientific Research, Bangalore 560012, India.

¹J.G. Bednorz and K.A. Muller, *Z. Phys.* **64**, 189 (1986).

²P. Kuiper, J. van Elp, G.A. Sawatzky, A. Fujimori, and D.M. de Leeuw, *Phys. Rev. B* **44**, 4570 (1991).

³Y. Takeda, R. Kanno, O. Yamamoto, M. Takano, Y. Bando, H. Akinaga, K. Takita, and J.B. Goodenough, *Mater. Res. Bull.* **25**, 293 (1990).

⁴J. Zaanen, G.A. Sawatzky, and J.W. Allen, *Phys. Rev. Lett.* **55**, 418 (1985).

⁵D.D. Sarma, H.R. Krishnamurthy, Seva Nimkar, S. Ramasesha, P.P. Mitra, and T.V. Ramakrishnan, *J. Phys.* **38**, L531 (1992); Seva Nimkar, D.D. Sarma, H.R. Krishnamurthy, and S. Ramase-

sha, *Phys. Rev. B* **48**, 7355 (1993).

⁶See also H.R. Krishnamurthy, C. Jayaprakash, S. Sarker, and W. Wenzel, *Phys. Rev. Lett.* **64**, 950 (1990); C. Jayaprakash, H.R. Krishnamurthy, S. Sarker, and W. Wenzel, *Europhys. Lett.* **15**, 625 (1991).

⁷The interaction between different planes of Ni-O_6 octahedral units along the c axis is neglected because two La layers intervene between them, making any such interaction very weak.

⁸J.C. Slater and G.F. Koster, *Phys. Rev.* **94**, 1498 (1954).

⁹J.B. Grant and A.K. McMahan, *Physica C* **162-164**, 1439 (1989).

¹⁰Of course one must ascertain whether terms other than those in model (1) are important in different A_2BO_4 systems. Examples of such terms include full multiplet interactions within the intra-atomic terms and extended Hubbard interactions.